Research Article | Vol. 25, No. 22 | 30 Oct 2017 | OPTICS EXPRESS 26853
Optics EXPRESS

O-band electrically injected quantum dot micro-ring lasers on on-axis (001) GaP/Si and V-groove Si

YATING WAN,[1,5] DAEHWAN JUNG,[1,5] JUSTIN NORMAN,[2,5] CHEN SHANG,[2] IAN MACFARLANE,[3] QIANG LI,[4] M. J. KENNEDY,[3] ARTHUR C. GOSSARD,[2,3] KEI MAY LAU,[4] AND JOHN E. BOWERS[2,3,*]

[1]*Institute for Energy Efficiency, University of California Santa Barbara, Santa Barbara, California, 93106, USA*
[2]*Materials Department, University of California Santa Barbara, Santa Barbara, California 93106, USA*
[3]*Department of Electrical and Computer Engineering, University of California Santa Barbara, Santa Barbara, California 93106, USA*
[4]*Department of Electronic and Computer Engineering, Hong Kong University of Science and Technology, Clear Water Bay, Kowloon, Hong Kong*
[5]*These authors contributed equally to this work*
[*]*bowers@ece.ucsb.edu*

Abstract: We report statistical comparisons of lasing characteristics in InAs quantum dot (QD) micro-rings directly grown on on-axis (001) GaP/Si and V-groove (001) Si substrates. CW thresholds as low as 3 mA and high temperature operation exceeding 80 °C were simultaneously achieved on the GaP/Si template template with an outer-ring radius of 50 μm and a ring width of 4 μm, while a sub-milliamp threshold of 0.6 mA was demonstrated on the V-groove Si template with a smaller cavity size of 5-μm outer-ring radius and 3-μm ring width. Evaluations were also made with devices fabricated simultaneously on native GaAs substrates over a significant sampling analysis. The overall assessment spotlights compelling insights in exploring the optimum epitaxial scheme for low-threshold lasing on industry standard Si substrates.

OCIS codes: (140.5960) Semiconductor lasers; (140.3948) Microcavity devices; (230.5590) Quantum-well, -wire and -dot devices.

References and links

1. A. E. Willner, R. L. Byer, C. J. Chang-Hasnain, S. R. Forrest, H. Kressel, H. Kogelnik, G. J. Tearney, C. H. Townes, and M. N. Zervas, "Optics and photonics: Key enabling technologies," in *Proceedings of the IEEE* (2012), pp. 1604–1643.
2. M. J. R. Heck and J. E. Bowers, "Energy efficient and energy proportional optical interconnects for multi-core processors: Driving the need for on-chip sources," IEEE J. Sel. Top. Quantum Electron. **20**(4), 1–12 (2014).
3. C. Zhang, S. Zhang, J. D. Peters, and J. E. Bowers, "8× 8× 40 Gbps fully integrated silicon photonic network on chip," Optica **3**(7), 785–786 (2016).
4. D. Liang, X. Huang, G. Kurczveil, M. Fiorentino, and R. G. Beausoleil, "Integrated finely tunable microring laser on silicon," Nat. Photonics **10**(11), 511–517 (2016).
5. G. Roelkens, L. Liu, D. Liang, R. Jones, A. Fang, B. Koch, and J. E. Bowers, "III-V/silicon photonics for on-chip and intra-chip optical interconnects," Laser Photonics Rev. **4**(6), 751–779 (2010).
6. M. A. Tran, T. Komljenovic, J. C. Hulme, M. J. Kennedy, D. J. Blumenthal, and J. E. Bowers, "Integrated optical driver for interferometric optical gyroscopes," Opt. Express **25**(4), 3826–3840 (2017).
7. C. Xiang, M. A. Tran, T. Komljenovic, J. Hulme, M. Davenport, D. Baney, B. Szafraniec, and J. E. Bowers, "Integrated chip-scale Si3N4 wavemeter with narrow free spectral range and high stability," Opt. Lett. **41**(14), 3309–3312 (2016).
8. Intel, "Intel Silicon Photonics 100G PSM4 Optical Transceiver Brief," https://www.intel.com/content/www/us/en/architecture-and-technology/silicon-photonics/optical-transceiver-100g-psm4-qsfp28-brief.html.
9. J.E. Bowers, "Evolution of Photonic Integrated Circuits," (2017).
10. D. Liang and J. E. Bowers, "Recent progress in lasers on silicon," Nat. Photonics **4**(8), 511–517 (2010).
11. Z. Zhou, B. Yin, and J. Michel, "On-chip light sources for silicon photonics," Light Sci. Appl. **4**, e358 (2015).

#305710 https://doi.org/10.1364/OE.25.026853
Journal © 2017 Received 29 Aug 2017; revised 6 Oct 2017; accepted 15 Oct 2017; published 18 Oct 2017

Optics EXPRESS

12. Z. Wang, A. Abbasi, U. Dave, A. D. Groote, S. Kumari, B. Kunert, C. Merckling, M. Pantouvaki, Y. Shi, B. Tian, K. V. Gasse, J. Verbist, R. Wang, W. Xie, J. Zhang, Y. Zhu, J. Bauwelinck, X. Yin, Z. Hens, J. Van Campenhout, B. Kuyken, R. Baets, G. Morthier, D. V. Thourhout, and G. Roelkens, "Novel light source integration approaches for silicon photonics," Laser Photonics Rev. **11**(4), 63 (2017).
13. Y. Arakawa and H. Sakaki, "Multidimensional quantum well laser and temperature dependence of its threshold current," Appl. Phys. Lett. **40**(11), 939–941 (1982).
14. D. Bimberg and U. W. Pohl, "Quantum dots: promises and accomplishments," Mater. Today **14**(9), 388–397 (2011).
15. A. Y. Liu, S. Srinivasan, J. Norman, A. C. Gossard, and J. E. Bowers, "Quantum dot lasers for silicon photonics," Photonics Res. **3**(5), B1–B9 (2015).
16. M. Tang, S. Chen, J. Wu, Q. Jiang, V. G. Dorogan, M. Benamara, Y. I. Mazur, G. J. Salamo, A. Seeds, and H. Liu, "1.3-μm InAs/GaAs quantum-dot lasers monolithically grown on Si substrates using InAlAs/GaAs dislocation filter layers," Opt. Express **22**(10), 11528–11535 (2014).
17. Y. Wan, Q. Li, A. Y. Liu, A. C. Gossard, J. E. Bowers, E. L. Hu, and K. M. Lau, "Optically pumped 1.3 μm room-temperature InAs quantum-dot micro-disk lasers directly grown on (001) silicon," Opt. Lett. **41**(7), 1664–1667 (2016).
18. A. Y. Liu, R. W. Herrick, O. Ueda, P. M. Petroff, A. C. Gossard, and J. E. Bowers, "Reliability of InAs/GaAs quantum dot lasers epitaxially grown on silicon," IEEE J. Sel. Top. Quantum Electron. **21**(6), 1900708 (2015).
19. S. Chen, W. Li, J. Wu, Q. Jiang, M. Tang, S. Shutts, S. N. Elliott, A. Sobiesierski, A. J. Seeds, I. Ross, P. M. Smowton, and H. Liu, "Electrically pumped continuous-wave III–V quantum dot lasers on silicon," Nat. Photonics **10**, 307–311 (2016).
20. J. Norman, M. J. Kennedy, J. Selvidge, Q. Li, Y. Wan, A. Y. Liu, P. G. Callahan, M. P. Echlin, T. M. Pollock, K. M. Lau, A. C. Gossard, and J. E. Bowers, "Electrically pumped continuous wave quantum dot lasers epitaxially grown on patterned, on-axis (001) Si," Opt. Express **25**(4), 3927–3934 (2017).
21. S. Chen, M. Liao, M. Tang, J. Wu, M. Martin, T. Baron, A. Seeds, and H. Liu, "Electrically pumped continuous-wave 1.3 μm InAs/GaAs quantum dot lasers monolithically grown on on-axis Si (001) substrates," Opt. Express **25**(5), 4632–4639 (2017).
22. A. Y. Liu, J. Peters, X. Huang, D. Jung, J. Norman, M. L. Lee, A. C. Gossard, and J. E. Bowers, "Electrically pumped continuous-wave 1.3 μm quantum-dot lasers epitaxially grown on on-axis (001) GaP/Si," Opt. Lett. **42**(2), 338–341 (2017).
23. D. Jung, J. Norman, M. J. Kennedy, C. Shang, B. Shin, Y. Wan, A. C. Gossard, and J. E. Bowers, "High efficiency low threshold current 1.3 μm InAs quantum dot lasers on on-axis (001) GaP/Si," Appl. Phys. Lett. under review.
24. Y. Wan, Q. Li, A. Y. Liu, W. W. Chow, A. C. Gossard, J. E. Bowers, E. L. Hu, and K. M. Lau, "Sub-wavelength InAs quantum dot micro-disk lasers epitaxially grown on exact Si (001) substrates," Appl. Phys. Lett. **108**(22), 221101 (2016).
25. J. E. Bowers, A. Y. Liu, D. Jung, J. Norman, A. C. Gossard, Y. Wan, Q. Li, K. M. Lau, and M. L. Lee, "InAs/GaAs quantum dot lasers on exact GaP/Si (001) and other templates," 2017.
26. Y. Wan, J. Norman, Q. Li, M. J. Kennedy, D. Liang, C. Zhang, D. Huang, Z. Zhang, A. Y. Liu, A. Torres, D. Jung, A. C. Gossard, E. L. Hu, K. M. Lau, and J. E. Bowers, "1.3 μm submilliamp threshold quantum dot micro-lasers on Si," Optica **4**(8), 940–944 (2017).
27. Y. Wan, J. Norman, Q. Li, M. J. Kennedy, D. Liang, C. Zhang, D. Huang, A. Y. Liu, A. Torres, D. Jung, A. C. Gossard, E. L. Hu, K. M. Lau, and J. E. Bowers, "Sub-mA threshold 1.3 μm CW lasing from electrically pumped micro-rings grown on (001) Si," in *CLEO: Applications and Technology 2017* (2017), paper JTh5C.3.
28. Q. Li, K. W. Ng, and K. M. Lau, "Growing antiphase-domain-free GaAs thin films out of highly ordered planar nanowire arrays on exact (001) silicon," Appl. Phys. Lett. **106**(7), 072105 (2015).
29. Q. Li, Y. Wan, A. Y. Liu, A. C. Gossard, J. E. Bowers, E. L. Hu, and K. M. Lau, "1.3-μm InAs quantum-dot micro-disk lasers on V-groove patterned and unpatterned (001) silicon," Opt. Express **24**(18), 21038–21045 (2016).
30. A. Y. Liu, C. Zhang, A. Snyder, D. Lubyshev, J. M. Fastenau, A. W. K. Liu, A. C. Gossard, and J. E. Bowers, "MBE growth of P-doped 1.3 μm InAs quantum dot lasers on silicon," J. Vac Sci. Technol B **32**(2), 02C108 (2014).
31. W. W. Chow, A. Y. Liu, A. C. Gossard, and J. E. Bowers, "Extraction of inhomogeneous broadening and nonradiative losses in InAs quantum-dot lasers," Appl. Phys. Lett. **107**(17), 171106 (2015).
32. O. Shchekin and D. Deppe, "1.3 μm InAs quantum dot laser with T_0= 161 K from 0 to 80 C," Appl. Phys. Lett. **80**(18), 3277–3279 (2002).

1. Introduction

There has been a lot of research over the last couple of decades to manage the tidal wave of data demand for efficient and cost-effective transmission [1, 2]. Fiber optics has replaced copper interconnects in long-haul and metro telecommunication links and a similar trend in data interconnect links is happening at increasingly short length scales down to 1 m [3–7]. Highly integrated 100-Gbps transceivers are already being shipped in volume and proposals

Optics EXPRESS

for the next generation at 400 Gbps are evolving [8]. This photonic revolution started with integration on InP but higher volumes are possible by transforming to manufacturing using low-cost, large-area silicon (Si) substrates combined with high gain III-V epitaxial materials [9].

Monolithic integration of III-V materials on Si by direct growth used to be inferior to other integration schemes due to the high sensitivity of semiconductor lasers to crystalline defects from heteroepitaxy [10]. However, recent research has placed great focus on this field resulting in several techniques to accommodate the material differences and mitigate the growth defects [11, 12]. Many traditional complementary metal-oxide-semiconductor (CMOS) foundries are now exploring the epitaxial growth of III-V on Si as a "More-than-Moore" technology to extend the gate length scaling limits of transistors [9]. The same technology is synchronously leveraged for photonics with recent advances in utilizing dense and spatially isolated quantum dots (QDs) to circumvent crystal defects in heteroepitaxy [13–17]. High performance InAs QD lasers on Si substrates are already showing decent performance with much improved lifetimes over any other kind of epitaxial lasers on Si [18, 19]. Miscut Si substrates have traditionally been employed to avoid antiphase-domain formation while growing polar III-V materials on non-polar Si substrates, but recent breakthroughs with on-axis (001) CMOS compatible Si substrates with no germanium or offcut have demonstrated comparable or better performance [20–24].

Recently, we employed on-axis GaP/Si and V-groove Si substrates to demonstrate high performance Fabry-Perot (FP) QD laser diodes with output powers of more than 100 mW and continuous wave (CW) threshold currents of ~30 mA at room temperature [20, 22, 25]. To further achieve easily manufacturable on-chip Si light sources having dense integration and low power consumption, we combined the advantages of a QD gain region with the small volume and discrete modes of a micro-ring cavity geometry. Using such a structure, electrically-driven lasers with record low, sub-milliamp threshold currents and continuous wave operation at 100 °C were demonstrated on the V-groove Si template [26, 27]. The discrete number of modes and small volume of the micro-rings allow much lower lasing thresholds compared to the larger FP geometries. The carrier localization possible with QDs provides a notable advantage in scaling to small dimensions through reduced sidewall recombination. The exceptional lasing performance achieved in V-groove Si is a motivation to explore the approach for whispering gallery mode (WGM) cavity lasers on on-axis Si that use a GaP/Si template.

In this paper, we demonstrate room temperature (RT) continuous wave (CW) operation of 1.3-μm InAs quantum-dot micro-ring lasers using a GaP/Si template, and present their comparisons to V-groove Si templates and native GaAs substrates. A systematic study of the lasing characteristics of the electrically driven micro-ring lasers has been conducted. The statistical significance of the study is to establish a clear correlation between the buffer material quality and device characteristics. Here, devices with identical designs on the three templates were simultaneously fabricated. More than 30 lasers on each template were characterized for their light-current-voltage (L-I-V) and temperature characteristics. A clear monotonic decrease of the threshold current with the scaling of the cavity size and a clear difference in performance on the three templates can be seen. The analysis here presents a set of important, compelling new insights into the correlations between device characteristics and crystalline quality of the epitaxial template structures on Si.

2. Experiments and results

In this study, Si (001) substrates without any specified offcut angle have been used for growth and antiphase boundary-free epilayers have been achieved for both templates. The GaP/Si template was obtained from $NAsP_{III-V}$, GmbH and regrowth of the GaAs template was performed using molecular beam epitaxy (MBE), similar to the method outlined in [22]. The surface morphology of the metal-organic chemical vapor deposition (MOCVD) grown V-

Optics EXPRESS

groove Si template in this manuscript has been improved compared with the previous results [28, 29]. With fifteen periods of Al0.3Ga0.7As/GaAs (5/5 nm) superlattice inserted, the root-mean-square (RMS) roughness in a 10 × 10 μm^2 atomic force microscopy (AFM) scan has decreased from 1.9 nm to 0.8 nm. Prior to laser growth, the two templates were characterized with electron channeling contrast imaging (ECCI), The ECCI images and schematic diagram of the two on-axis Si templates are shown in Figs. 1(a) and 1(b), respectively. Pinpoints of bright contrast indicate threading dislocations intersecting the surface. By counting the defects, threading dislocation density of ~7 × 10^{7}cm^{-2} and 2.1 × 10^8 cm^{-2} were calculated for the GaP/Si and V-groove Si substrates, respectively. Also, note that the islands seen in Fig. 1(a) are due to the islanding growth of the initial GaAs layer on the GaP/Si.

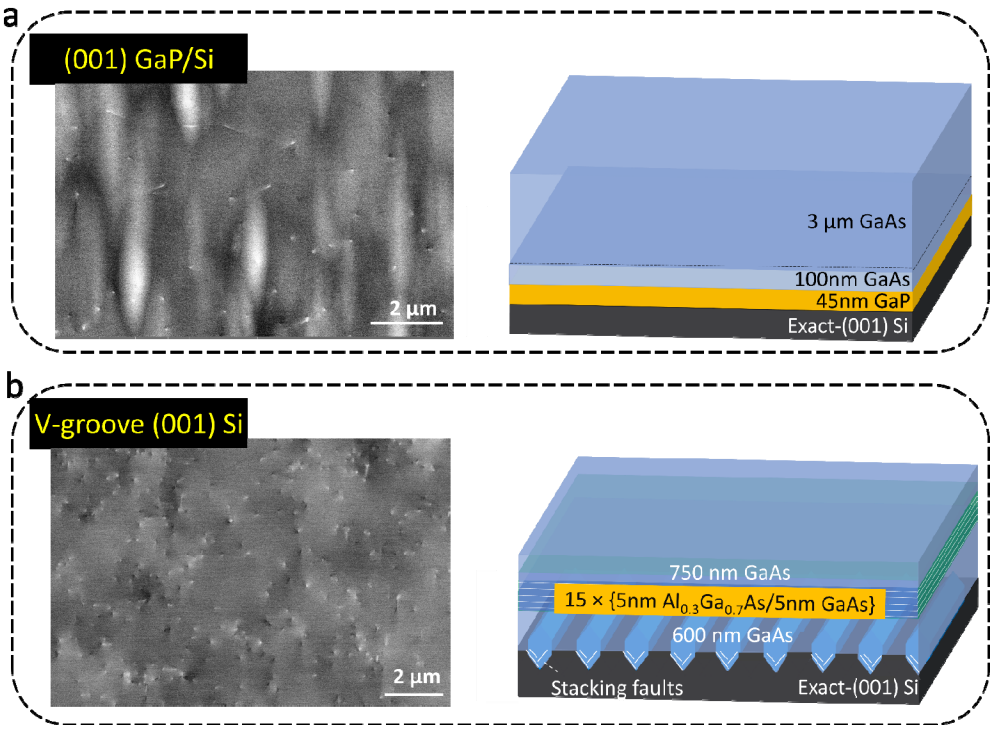

Fig. 1. ECCI images and schematic diagram of (a) the GaP/Si template and (b) the V-groove Si template.

Together with a native GaAs substrate, micro-ring laser structures containing a seven-layer InAs/InGaAs quantum dot-in-a-well (DWELL) active region were subsequently grown using MBE [30]. The high-quality QDs on Si (001) substrate was assessed through the growth of photoluminescence (PL) structures containing one embedded layer of QDs and one surface layer for AFM measurement of the dot density. A dot density of 5.2 × 10^{10} cm^{-2} was obtained from the AFM scan and a strong luminescence at 1285 nm with a full-width at half-maximum of 28 meV was obtained from PL measurements [23]. The final epitaxial structure includes a 1.4-μm *n*-type lower $Al_{0.4}Ga_{0.6}As$ cladding layer, a 20-nm gradient layer, a 30-nm $Al_{0.2}Ga_{0.8}As$ guiding layer, a standard undoped seven-layer DWELL laser active structure separated by 50-nm GaAs spacer layers, a second 30-nm $Al_{0.2}Ga_{0.8}As$ guiding layer, 20-nm gradient layer, and a 1.4-μm *p*-type upper $Al_{0.4}Ga_{0.6}As$ cladding layer, and finally a 300 nm highly *p*-type doped GaAs contacting layer [26]. Ring lasers with varying outer-ring radius were fabricated simultaneously from the as-grown materials on the three templates. A schematic of the micro-ring is shown in the lower inset in Fig. 2(a). We used an i-line (365

Optics EXPRESS

nm) step-and-repeat exposure tool for lithographic patterning to provide high resolution and critical alignment for definition of the electrode metallization in the micron-scale cavity. A special GaAs etching recipe was developed to form 4 μm-tall mesas with a straight etching profile and smooth sidewall surfaces. A Pd/Ti/Pd/Au *p*-contact was deposited on top of the etched ring mesa, and a Pd/Ge/Au *n*-contact metal was deposited on the exposed *n*-GaAs layers with 60s annealing at 300°C to achieve Ohmic contacts.

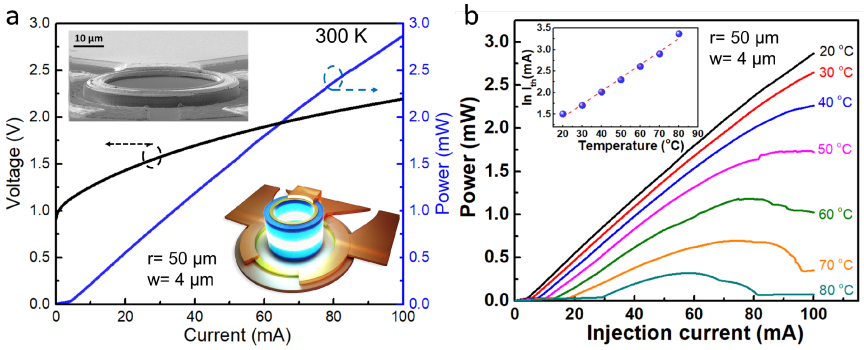

Fig. 2. (a) L-I-V curve at room temperature and (b) L-I curves as a function of temperature for a micro-ring laser with a radius of 50 μm and a ring width of 4 μm under CW operation on the GaP/Si template. Inset in (a): SEM image and 3D schematic of the fabricated micro-ring laser. Inset in (b): natural logarithm of threshold current versus temperature. A characteristic temperature, T_0, of 33 K was extracted by linear fitting.

A fabricated device is shown in the cross-sectional view scanning electron microscope (SEM) image in the upper inset of Fig. 2(a). The devices were probed under CW electrical injection. Figure 2(a) shows a representative room-temperature L-I-V curve of a micro-ring laser with an outer-ring radius of 50 μm and a ring width of 4 μm on the GaP/Si template. The optical power was measured by collecting radiation out-coupling from the micro-laser cavity through an integrating sphere at the side. CW thresholds as low as 3 mA and output powers exceeding 3 mW were simultaneously achieved. The low threshold current density (J_{th}) of 0.25 kA/cm^2 outperforms the best reported FP laser epitaxially grown on Si (001) substrates, despite of the high aspect ratio of sidewall/active region volume (~0.0768 μm^{-1}) in this small-footprint micro-ring structure [20–22]. The external differential quantum efficiency was extracted to be 0.03. A plot of the light-current (L-I) curves versus temperature for the same device is shown in Fig. 2(b). CW lasing is maintained to temperatures above 80 °C. By plotting the natural logarithm of threshold current as a function of temperature in the inset in Fig. 2(b), the characteristic temperature, T_0, was extracted to be ~33 K through linear fitting. The extracted T_0 here was an underestimated value considering the effect of self-heating under CW excitation. Nevertheless, this value compares favorably to that of a recently reported FP laser epitaxially grown on Si (001) under pulsed injection (32 K) [21].

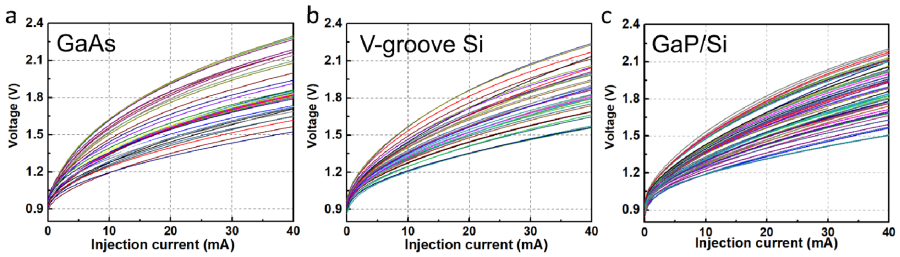

Fig. 3. Room-temperature CW current–voltage characteristics for (a) the GaAs substrate; (b) the V-groove Si template; and (c) the GaP/Si template.

Optics EXPRESS

A statistical analysis of a sampling of micro-rings was performed to reach a fair comparison between the different substrates. I–V characteristics between devices from the three separate wafers on GaAs, V-groove Si and GaP/Si substrates are presented in Figs. 3(a)-3(c), respectively. More than 30 samples were measured, and the measurement shows similar values of series resistance on the three different templates. This indicates the doping levels and metallization conditions were nominally identical for the three samples. Furthermore, scanning electron microscope (SEM) observations were conducted right after ring mesa deep dry etching. Although process variations inevitably resulted in micro-rings with imperfect shapes, the sidewall of the rings exhibited roughness at a similar level from device to device. These measurements assure that the simultaneously fabricated micro-rings on the three wafers have nominally the same process conditions and the following comparisons of lasing characteristics should be indicative of differences in the templates.

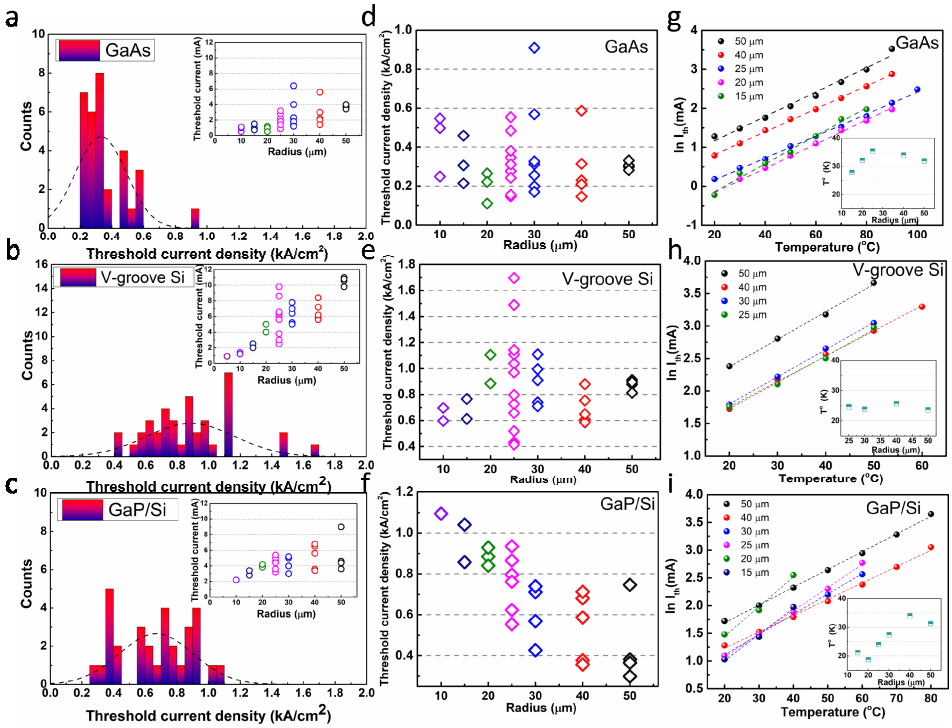

Fig. 4. A histogram of CW threshold current density at room temperature for (a) the GaAs substrate; (b) the V-groove Si template; and (c) the GaP/Si template. The dotted lines represent normal distribution curve of the data. Inset: Corresponding threshold currents plotted against outer-ring radius. The threshold current density is plotted against outer-ring radius for (d) the GaAs substrate; (e) the V-groove Si template; and (f) the GaP/Si template. Natural logarithm of threshold current versus stage temperature for micro-rings with various outer-ring radius on (g) the GaAs substrate; (h) the V-groove Si template; and (i) the GaP/Si template. The dotted lines represent linear fitting to the experimental data. Inset: the corresponding characteristic temperature as a function of the outer-ring radius.

Histograms of the threshold current density for a number of devices at room temperature on the three templates are presented in Figs. 4(a)-4(c). The average threshold current density of the micro-rings on the GaP/Si template (0.675 kA/cm^2) yielded a ~2-fold increase compared to devices on the native GaAs substrate (0.325 kA/cm^2), and was comparable to that of devices on the V-groove Si template (0.875 kA/cm^2). The 2-3 times higher threshold current density on the two Si templates compared to the native substrate originates from non-radiative recombination. Better intrinsic performance of the heteroepitaxially grown lasers

Optics EXPRESS

could be achieved by reducing nonradiative losses via enhancing the quality of the GaAs films on Si, as well as by improving the size uniformity of the quantum dots [31]. Insets in Figs. 4(a)-4(c) present the corresponding threshold currents as a function of the outer-ring radius for the three templates. Despite certain discrepancies in performance, a clear monotonic decrease of the threshold current with the scaling of the cavity size was observed over the entire range of ring radius studied for all three samples. This implies reduced sidewall recombination and constrained lateral carrier diffusion due to the excellent carrier confinement within the QDs. The threshold of the best working device on the V-groove Si template (0.6 mA) was achieved on a micro-ring with an outer-ring radius of 5 μm and ring width of 3 μm. The smallest lasing device found on the GaAs substrate (0.5 mA) and GaP/Si (2.2 mA) possesses a larger outer-ring radius of 10 μm and ring width of 4 μm due to probe metal shorts for smaller rings. The threshold currents fall into the range of 0.5-6.4 mA,0.6-11 mA, and 2.2-9 mA, for micro-rings on the GaAs substrate, the V-groove Si template, and the GaP/Si template, respectively. The low-threshold laser operation under room temperature CW electrical injection presents solid evidence of the high optical quality of the III–V crystals monolithically grown on Si, for both the GaP/Si and V-groove Si templates. Threshold current densities with different outer-radius for the GaAs substrate, the V-groove Si template, and the GaP/Si template are presented in Figs. 4(d)-4(f). The larger cavity rings with smaller aspect ratio of sidewall/active region volumes possess a general trend of decreased J_{th}. The lowest value of J_{th} obtained for micro-rings on the GaAs substrate, the V-groove Si template, and the GaP/Si template is 0.11 kA/cm^2, 0.41 kA/cm^2, 0.25 kA/cm^2, respectively.

Temperature characteristics of the micro-rings were studied by testing the devices at various heatsink temperatures and analyzing their L-I characteristic under CW injection. The data range is restricted to 20-100 °C, limited by the thermoelectric heater. The natural logarithm of threshold versus temperature is plotted for micro-rings with various outer-ring radius in Figs. 4(g)-4(i). Through linear fitting, the corresponding T_0 was extracted and summarized in the insets in in Figs. 4(g)-4(i). The T_0 results fall into the range of 27-35 K, 25-26 K, and 20-40 K, for micro-rings on the GaAs substrate, the V-groove Si template, and the GaP/Si template, respectively. The T_0 for micro-ring lasers on the two compliant Si substrates are quite close to that of the lasers on the native substrates. It is anticipated that the well-established strategies using modulation *p*-doping of the QDs and hard soldering the laser to a high-thermal-conductivity heatsink will further reduce the temperature sensitivity and improve the extraction of heat from the active region [32].

Comparing the results of lasers grown on the two on-axis Si (001) substrates, both the temperature characteristics and the threshold currents of micro-rings on GaP/Si templates are better than that of the lasers on the V-groove Si templates, but not as much as 3-fold of discrepancy in threading dislocation density measured by ECCI. This further demonstrates the somewhat forgiving nature of QDs to withstand defects. Another important aspect of integrating active devices on Si is that the Si substrate cannot only be used as a substrate carrier but also be used as waveguiding material because of the low optical material losses. Both the compliant Si templates used in this work do not include any absorptive germanium buffers, and the V-groove Si template has a 1.7 μm thinner buffer thickness compared to that of the GaP/Si template. The thin and low-loss buffer saves growth time, allows easier coupling from the laser active regions to Si waveguides and suggests potential opportunity to be incorporated in the well-developed silicon-on-insulator (SOI) technology in Si photonics. Moreover, the smaller RMS roughness of the V-groove Si (0.8 nm) than that of the GaP/Si (2.48 nm) is beneficial for subsequent device fabrication.

3. Conclusions

In conclusion, electrically injected micro-ring lasers were demonstrated on (001) Si substrates with low thresholds using different epitaxial schemes. A comprehensive comparison of the lasing characteristics was made in devices with the same active structures and geometries but

Optics EXPRESS

fabricated on different GaAs-on-Si templates. Ultimately the established GaAs-on-Si templates can be visualized as virtual III-V substrates and entire photonic integrated circuits could be fabricated from the epitaxially deposited III-V layers, allowing for scaling photonic integrated circuits to 300 mm and even 450 mm diameter wafer size in high volume applications. Currently, the GaP/Si template possesses three-fold lower defect densities while the V-groove Si is advantageous in smoother surface and thinner buffer layers. Both growth techniques are improving rapidly to meet the demands for low defect density, smooth growth surface, thin buffer layers, and most importantly, the ability to fabricate high performance devices at the lowest lifecycle cost and the highest yield.

Funding

This work was supported by the Advanced Research Projects Agency-Energy (ARPA-E) (DE-AR0000672), Research Grants Council of Hong Kong (RGC) (No 16212115), Innovation Technology Fund of Hong Kong (ITS/320/14).

Acknowledgment

The authors would like to thank AIM and SUNY Poly for providing the initial nano-patterned Si substrates, Mike Haney, Di Liang, Alan Liu, Minh Tran, Chao Xiang, Chong Zhang, and the UCSB nanofabrication clean room staff for helpful discussions and assistance.